

Electronic and molecular structure of 2-phenyl-3,3-dimethyl-3*H*-indole molecular fluorescence probe and the molecular structure of its dimer¹

M. Belletête, F. Brisse*, G. Durocher*, D. Gravel*, A. Héroux, A. Popowycz

Département de Chimie, Université de Montréal, C.P. 6128, Succ. A, Montréal, Que., H3C 3J7, Canada

(Received 1 February 1993)

Abstract

Crystallographic measurements as well as AMPAC and INDO/S calculations were performed on 2-phenyl-3,3-dimethyl-3*H*-indole (**1**). This fluorescent molecular probe was shown to dimerize in the solid and the X-ray structure shows that the dimer consists of two monomers linked by covalent bonds between the nitrogen atom (N1) of one molecule to the carbon atom C2 of the other molecule, and vice versa, thus forming a four-membered ring. It was observed that the dimer of **1** is labile in the presence of traces of acid and reverts back to the monomer. It is shown that AMPAC, while predicting good bond distances and angles, failed to predict the correct dihedral angle between the Ph_c ring and the indolic moiety. The semiempirical INDO/S method coupled to absorption and fluorescence spectral data in more than 18 non-polar, polar aprotic and/or protic solvents showed that the Ph_c ring should librate within a range of about 20° around the equilibrium dihedral angle of approximately 45° at room temperature in the ground electronic state of the molecule. This libration is responsible for the fact that the fluorescence quantum yields (ϕ_F) and lifetimes (τ_F) of **1** vary from 2.4×10^{-4} to 0.12 and from 1 to 520 ps, respectively, in the various solvents investigated as a result of viscosity dependent fast internal conversion. Rates of internal conversion are shown to be dependent upon the bulk viscosity of the solvent as opposed to the microviscosity (free volume effect of the solvent), so that the Förster–Hoffmann mechanism ($\phi_F = Ce^{2/3}$) with an identical value of *C* applies in all solvents. This molecule may then be regarded as an excellent viscosity probe for heterogeneous systems and polymers in a very large range of viscosities.

Introduction

Recent progress in the elucidation of the electron transfer (ET) mechanism in various fields of photochemistry and photobiology is partly owing to remarkable advances in experimental methods such as ultrafast laser spectroscopy [1]. Our research group has been involved recently in the study of intramolecular ET rates in bridged systems of the type carbazole donors–spacers–poly-

nitrofluorene acceptors [2]. These bichromophores were attached, as pendant groups, to polymeric chains which show good photoconductivity. A second type of ET reactions, that is, intermolecular charge separation reactions, studied by fluorescence quenching in the stationary state and from analysis of the transient effect in the fluorescence decay curve [1], were also studied in a series of substituted carbazoles and tocopherols in order to correlate the solvent reorganization energies in the Marcus–Hush theory to some experimental solvent parameters [3]. However, a third type of ET reactions between chromophores separated by one σ bond only (ref. 1, p. 133) has recently given

* Corresponding authors.

¹ This paper is dedicated to the honor of our colleague and friend, Emeritus Professor Camille Sandorfy.

rise to the molecular fluorescence probing technique [4–8]. The probes have been used successfully to study molecular organization and dynamics in macromolecules [4] and organized assemblies such as proteins [5], micelles [6], inverted micelles [7], lipid bilayers [4,5] and solid polymers [8]. Probes containing the dimethylamino group as an electron donor have increased in popularity because the ET dynamics are very fast and can exceed the solvation rates in some particular solvents, indicating that the intramolecular vibrational modes entirely control the promotion of ET in these systems [9]. Moreover, these probes sometimes give rise to the well-known twisted intramolecular charge transfer (TICT) states [10]. In these cases, the probes show a large decrease in fluorescence yield with increase in the polarity of the environment.

In the last few years we have managed to design and synthesize in our laboratory [11], dimethylamino probes which do not give rise to any TICT states, i.e. probes that show little difference between their ground and first relaxed singlet excited electronic state geometries. Consequently, their fluorescence yields and lifetimes strongly increase with the polarity of environments following an increase in charge delocalization and in the localized excited state dipole moment. The probe, 2-[*p*-(dimethylamino)phenyl]-3,3-dimethyl-3*H*-indole (DM3H), proved to be very sensitive to the polarity of interfaces which allowed us to probe the micropolarity of AOT inverted micelles [7]. It was shown that the semiempirical calculation method AMPAC-AM1 predicts a ground state geometry of DM3H very similar to that obtained from the X-ray crystallographic investigation, while INDO/S calculates transition energies, and ground- and excited-state dipole moments corresponding to those observed in the absorption spectrum in the vapor phase and to the dipole moments obtained from spectral shift data, respectively [12].

These calculations have indicated that the dimethylanilino ring (Ph_c) has a certain freedom of rotation within the kT energy barrier at room temperature in both S₀ and S₁ states so that the

photophysical behavior of these 3*H*-indole molecules becomes very sensitive to small chemical substitution (esterification in the para position of the indole ring or even only hydrogen substitution of a methyl group in the dimethylanilino moiety) [13] or to protonation on the various basic centers of the molecule [14]. The X-ray structure of all these substituted 3*H*-indoles has been obtained [15] and will be the object of a further publication. In non-polar media, the fluorescence lifetime (τ_F) and the fluorescence quantum yield (ϕ_F) of these molecules were found to vary with solvent viscosity according to the Förster–Hoffmann (FH) relationship: ϕ_F (or τ_F) = $C\eta^{2/3}$ [13,16]. But, just like for DM3H, in these various 3*H*-indole compounds in polar protic and/or aprotic solvents, the librational movement of the anilino moiety is much reduced so that the FH relationship can no longer apply in these environments precluding these molecules from becoming generalized viscosity probes even though they are good polarity probes [13]. By eliminating all substituent groups on the phenyl and indolic rings (2-phenyl-3,3-dimethyl-3*H*-indole (1)) it has recently been shown to produce an excellent viscosity probe in all apolar, polar protic and polar aprotic environments [17]. The FH relationship with an identical value of C in all homogeneous environments is observed so that 1 becomes an excellent viscosity probe for heterogeneous systems and polymers in a very large range of viscosities.

It was the purpose of this study to obtain more insight into the molecular and electronic structure of this powerful viscosity probe and also into the molecular structure of its dimer. Synthesis, X-ray data, molecular semi-empirical calculations and spectroscopic data are discussed.

Experimental

Melting points were determined using a Büchi silicone oil bath apparatus and were not corrected. Infrared spectra were recorded in KBr pellets using either a Perkin-Elmer 710B or a Perkin-Elmer 783 instrument. Signal positions are

given in wavenumbers (cm^{-1}) using the 1601 cm^{-1} band of polystyrene as reference.

NMR spectra were recorded on a Varian VXR-300 spectrometer using deuteriochloroform (CDCl_3) as solvent, unless otherwise specified. Chemical shifts (δ) are expressed in parts per million (ppm) with respect to tetramethylsilane (TMS) used as internal standard. Coupling constants are reported in hertz (Hz). The analysis of the resolved parts of the spectra were done by first-order approximation. The following notation is used to report the various signals appearing in the spectra: s for singlet, d for doublet, t for triplet, q for quartet, and m for multiplet. The ^{13}C NMR spectra reported were also recorded on a Varian VXR-300 (75.4 MHz) instrument. The solvent used, unless otherwise specified, was deuteriochloroform (CDCl_3). Chemical shifts (δ) are reported in parts per million (ppm) with respect to tetramethylsilane. Information concerning the "distortionless enhancement by polarization transfer" (DEPT) is also reported using the following notation: (+) positive signal for a primary or tertiary carbon atom, and (–) negative signal for a secondary carbon atom; absence of a (+) or (–) sign indicates a quaternary carbon atom.

Low resolution mass spectra were taken in the chemical ionization mode on an AEI MS-902 spectrometer. High resolution spectra were recorded in the electron impact mode on the same instrument.

Thin layer chromatography (TLC) was done on glass supported (0.5 mm thick) Kieselgel 60F₂₅₄ (Merck) plates and detection was done by direct visualization under UV light or dipping in a phosphomolybdic or potassium permanganate solution followed by heating to approximately 200°C on a hot-plate. Finally, flash chromatography was done on silica gel (Merck 60, 230 to 400 mesh) using the optimized method of Still et al. [18].

Materials

Synthesis and purity of 2-phenyl-3,3-dimethyl-3H-indole (1)

In a procedure slightly different from those

reported previously [19–21], a mixture of 5.017 g (33.90 mmol) of isobutyrophenone and 3.760 g (34.81 mmol) of phenylhydrazine was heated to 150°C under stirring for 1 h. Glacial acetic acid (10 ml) was then added to the resulting oil and the mixture heated to reflux for 4 h. The resulting reaction mixture was then diluted with water (50 ml) and basified with a saturated solution of sodium bicarbonate. The alkaline solution was copiously extracted with ether and the organic phases combined, dried over anhydrous sodium sulfate, filtered and evaporated under vacuo.

The residue was flash chromatographed, using dichloromethane to yield 5.152 g (23.3 mmol) (69%) of the desired indole derivative as an oil. The latter, after recrystallization from petroleum ether ($50\text{--}110^\circ\text{C}$), yields large colorless crystals: m.p. $39\text{--}41^\circ\text{C}$ (lit.) (refs. 19–21, always reported as an oil); rf (dichloromethane) 0.30; IR (KBr), 3080, 2980, 2940, 2860, 1660, 1620, 1490, 1470, 1455, 1445, 1390, 1260, 1000, 980, 765, 750 and 690 cm^{-1} ; ^1H NMR (300 MHz, CDCl_3), δ 1.60 (s, 6H), 7.24–7.26 (m, 1H), 7.28–7.40 (m, 2H), 7.47–7.51 (m, 3H), 7.69 (d, $J = 7.7\text{ Hz}$, 1H), 8.13–8.16 (m, 2H); ^{13}C NMR (300 MHz, CDCl_3), δ 24.58 (+), 53.38, 120.71 (+), 120.75 (+), 125.68 (+), 127.57 (+), 128.12 (+), 128.42 (+), 130.34 (+), 133.14 (+), 147.42, 152.42, 183.05; MS (CI), $M^+ = 221$; HRMS (EI), calculated for $\text{C}_{16}\text{H}_{15}\text{N}$ was 221.1204, found 221.1209.

Preparation of the dimer of 3,3-dimethyl-2-phenyl-3H-indole

In a small pyrex sample vial, 0.184 g (0.832 mmol) of finely crushed 3,3-dimethyl-2-phenyl-3H-indole was irradiated for 24 h in a Rayonet merry-go-round equipped with eight 350 nm lamps. The resulting solid was recrystallized from dichloromethane/hexane to yield 72 mg (0.16 mmol) (39%) of the dimer. M.p., $192\text{--}193^\circ\text{C}$; rf, reverts to monomer on silica gel plates upon elution with dichloromethane; IR (KBr), 3080, 3010, 2960, 2930, 1600, 1580, 1450, 1460, 1380, 1360, 1270, 1260, 1220, 1100, 1050, 1025, 1020, 1000, 750 and 710 cm^{-1} ; ^1H NMR (300 MHz,

CDCl₃, filtered over basic alumina), δ 0.72 (S, 6H), 1.79 (S, 6H), 6.82 (d, $J = 4.44$ Hz, 4H), 6.98–7.20 (m, 10H), 7.23 (d, $J = 7.69$ Hz, 2H), 7.66 (d, $J = 7.69$ Hz, 2H); ¹³C NMR(300 MHz, CDCl₃, filtered over basic alumina), δ 27.95 (+), 30.86 (+), 49.90, 77.10, 101.80, 121.34 (+), 123.14 (+), 123.74 (+), 125.43 (+), 125.88 (+), 126.61 (+), 127.28 (+), 128.10 (+), 128.96 (+), 137.60, 146.01, 146.71.

Purification of solvents for spectroscopic studies

All solvents used were purified following methods already described [7,12,13,17].

X-ray diffraction analyses

Single crystals of the compounds, suitable for X-ray diffraction, were obtained by slow evaporation from a petroleum ether or toluene solution. The crystals were mounted on an Enraf-Nonius CAD-4 diffractometer. The unit cell dimensions, obtained first from X-ray films, were confirmed and determined later with greater accuracy from 25 well-centered reflections in the range of $40^\circ < 2\theta < 50^\circ$. In both cases the graphite monochromatized CuK α radiation ($\lambda = 1.54178$ Å) was used. Crystal data of interest are presented in Table 1.

The orientation of the crystals was monitored every 200 measurements, while the intensities of the standard reflections were checked every hour. The diffracted intensities were placed on a common scale, then corrected for Lorentz and polarization effects but not for absorption because the absorption coefficients were small [22–25]. The structures were solved by direct methods using the MULTAN 80 set of programs. A block-diagonal least-squares procedure was used for the refinement of the atomic coordinates and the isotropic temperature factors. After convergence, the least-squares refinement was concluded with anisotropic temperature factors for the non-hydrogen atoms. The hydrogen atom positions were all revealed in subsequent difference Fourier syntheses. They were included in the refinement process with isotropic temperature factors. The details of the

Table 1

Crystal data for the monomer and the dimer derived from the 3*H*-indole

	Monomer	Dimer
Formula	C ₁₄ H ₁₅ N	C ₃₂ H ₃₀ N ₂
MW	231.30	442.60
M.p. (°C)	43–44	192–193
Crystal system	Orthorhombic	Monoclinic
Space group	<i>Pbca</i>	<i>P2₁/c</i>
<i>a</i> (Å)	11.761(6)	16.361(7)
<i>b</i> (Å)	15.073(5)	10.602(3)
<i>c</i> (Å)	14.094(5)	14.882(5)
α (deg)	90	90
β (deg)	90	109.73(3)
γ (deg)	90	90
<i>V</i> (Å ³)	2498.5(4)	2428.9(4)
<i>Z</i>	8	4
<i>d_c</i> (g cm ⁻³)	1.17	1.210
μ (Cu) (cm ⁻¹)	4.87	5.01
<i>F</i> (000)	944	944
<i>T</i> (°C)	-120	23

data collections and the structure refinements are presented in Table 2.

The refinement, based on *F* values, was carried out by minimizing the function $\sum_w (|F_o| - |F_c|)^2$ [26]. The weights were derived from the counting statistics, $w = 1/\sigma^2(F)$. The scattering factors for the oxygen, nitrogen and carbon atoms were taken from Cromer and Mann [27] while those for the hydrogen atoms were taken from Stewart et al. [28].

Semiempirical calculations

The geometry optimization in the electronic ground state was done by first using the MM2 force field of the program MODEL to generate the Cartesian coordinates [29]. A more precise geometry optimization was then obtained using the AM1 Hamiltonian of the AMPAC program which consists of an improved parameterization for the MNDO Hamiltonian [30]. The ground state and transition energies together with the dipole moments were calculated within the framework of the semi-empirical all-valence INDO method including configuration interaction (CI) [31], as already described [12].

Table 2
Summary of the data collections and structure refinements

	Monomer	Dimer
Crystal size (mm)	0.23 × 0.30 × 0.32	0.15 × 0.20 × 0.27
Radiation (Å)	CuK α 1.54178	CuK α 1.54178
Scan mode	ω	ω
Scan width (deg)	(0.80 + 0.40 tan θ)	(0.80 + 0.40 tan θ)
2 θ_{\max} (deg)	140	140
Octants measured	$hk \pm 1$	$hk \pm 1$
Maximum fluctuation of reference reflections (%)	3.0	3.0
No. of measured reflections	2343	4335
No. of observed reflections	1979	2671
$I_{\text{obs}} \geq k\sigma(I), k$	1.95	1.95
R^a	0.044	0.066
R_w	0.046	0.060
S	3.309	2.118
Residual electron density ($e \text{ \AA}^{-3}$)	0.15, -0.21	0.21, -0.22
Maximum and average values of (Δ/σ)	0.31, 0.08	0.22, 0.03

^a $R = \Sigma||F_o| - |F_c||/\Sigma|F_o|$, $R_w = [\Sigma_w(|F_o| - |F_c|)^2/\Sigma_w F_o^2]^{1/2}$ and $S = [\Sigma_w(|F_o| - |F_c|)^2/(m - n)]^{1/2}$, where m is the number of observed reflections and n is the number of refined variables.

Spectroscopic Instrumentation

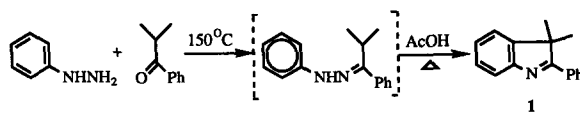
The absorption spectra were recorded on a Philips PU8800 UV/VIS spectrophotometer already described [7,12]. Excitation spectra and corrected fluorescence spectra were measured on a new Spex Fluorolog-2 spectrofluorometer with an F2T11I special T-shape configuration. Fluorescence quantum yields were measured in non-polar solvents by reference to the known value ($\phi_F = 0.025$) for DM3H in methylcyclohexane [32]. For the measurements in aprotic and protic solvents, the value ($\phi_F = 0.33$) for DM3H in ethanol was used as a reference [33]. The theoretical or natural radiative decay rate constants ($k_F^{(t)}$) were calculated from the well-known Strickler and Berg relationship [33,34]. Fluorescence lifetimes in glycerol have been obtained from a multiplexed time-correlated single-photon counting fluorimeter (Edinburgh Instruments, Model 299T) already described [2]. Lifetimes of molecule 1 in all other homogeneous media were too short to be measured, even with our synchronously pumped cavity dumped rhodamine 6G dye laser coupled to a microchannel plate

detector where the time resolution is approximately 20–30 ps [13].

Results and discussion

Synthesis of 2-phenyl-3,3-dimethyl-3H-indole and its dimer

The monomer was prepared using a procedure slightly different from those reported in the literature for the preparation of the same compound [19–21] (see Scheme 1). In the procedure of Evans et al. [19], the phenylhydrazone derivative of isobutyrophenone is prepared and then isolated. In a second step, it is submitted to cyclization to the corresponding 3H-indole derivative by refluxing in glacial acetic acid. These authors, as well as the other groups who reported preparations of the monomer, isolated the final



Scheme 1.

3*H*-indole derivative by fractional distillation (b.p. 146°C, 0.4 mmHg) and report the product as an oil.

In our case, the preparation was done in a one-pot procedure, i.e. without isolation of the intermediate phenylhydrazone and, probably more importantly, the final 3*H*-indole was purified by flash chromatography to yield a crystalline material, m.p. 39–41°C, after recrystallization from petroleum ether.

The dimer was obtained for the first time, quite serendipitously. Indeed, a solution of the monomer in toluene was recrystallized to obtain a single crystal for X-ray diffraction purposes. Upon analysing the data, however, it was realized that the compound was a dimer, in spite of the fact that the compound originally prepared had been shown by UV and NMR spectroscopy to be the desired 3*H*-indole derivative. It was then hypothesized, and later demonstrated (see below), that the solid melting at 39–41°C is indeed the desired compound, but that it may inadvertently have been exposed to sunlight prior to being submitted for X-ray structure analysis. Then, upon recrystallization in toluene, a single crystal was obtained which proved to be that of the dimer.

This hypothesis was substantiated by attempting, without success at first, to dimerize the monomer by irradiation in solution at 350 nm. However, the dimer was then obtained by irradiation of the monomer in the crystalline state.

Thus, the dimer was prepared by irradiating finely crushed monomer in a sample pyrex tube at 350 nm, and the resulting solid recrystallized from dichloromethane/hexane to yield the dimer (m.p. 192–193°C). An interesting aspect of the dimer is its lability under acidic conditions. For instance, it reverts back to monomer on silica gel TLC plates upon elution with dichloromethane. This reversal to monomer can also be observed by NMR when one records the spectrum in CDCl₃ or even in CD₂Cl₂ but then the reversal is slower. The reversal to monomer was presumed to be due to the presence of traces of acid in the deuterated solvents and this was substantiated by filtering the

deuterated solvents over basic alumina prior to recording the spectrum.

Crystallographic investigation

The melting points of the two forms are very different, with values of 43–44°C and 192–193°C for the monomer and the dimer, respectively. Both compounds are very stable at room temperature but, because the melting point of the monomer is near room temperature, its X-ray intensity data collection was performed at –120°C. The refined atomic coordinates [22] and their standard derivations (e.s.d. values) are presented in Tables 3 and 4.

Monomer.

The density indicates that only one monomer molecule occupies the asymmetric unit. The atomic numbering adopted is shown in Fig. 1. The bond distances and bond angles are listed in Table 5. The geometrical features (bond distances and angles) observed in the monomer are comparable in all respects to the corresponding quantities reported for 2-[*p*-(dimethylamino)phenyl]-3,3'-dimethyl-3*H*-indole [12]. The 3*H*-indole group of atoms is coplanar, the only small deviation is

Table 3

Refined atomic coordinates ($\times 10^4$) and isotropic temperature factors $U_{\text{eq}} (\times 10^4 \text{ \AA}^2)$ for the monomer C₁₆H₁₅N:
 $U_{\text{eq}} = \frac{1}{3} \sum_i \sum_j U_{ij} a_i^* a_j^* a_i \cdot a_j$

Atom	x	y	z	U_{eq}
N1	994(1)	4252(1)	5435(1)	314
C2	100(1)	3842(1)	5751(1)	293
C3	–365(1)	3125(1)	5068(1)	326
C3a	484(1)	3226(1)	4273(1)	328
C4	602(2)	2787(1)	3413(1)	407
C5	1485(2)	3031(1)	2812(1)	435
C6	2238(2)	3709(1)	3065(1)	414
C7	2125(1)	4149(1)	3929(1)	372
C7a	1247(1)	3898(1)	4524(1)	310
C8	–367(1)	4069(1)	6695(1)	308
C9	218(2)	4694(1)	7259(1)	373
C10	–196(2)	4941(1)	8142(1)	449
C11	–1201(2)	4582(1)	8483(1)	451
C12	–1790(2)	3963(1)	7940(1)	426
C13	–1372(2)	3706(1)	7055(1)	374
C14	–270(2)	2184(1)	5510(1)	433
C15	–1583(2)	3312(1)	4712(1)	461

Table 4
Refined atomic coordinates ($\times 10^4$) and isotropic temperature factors U_{eq} ($\times 10^3 \text{ \AA}^2$) for the dimer $C_{32}H_{30}N_2$

Atom	x	y	z	U_{eq}
<i>Molecule I</i>				
N1	-58(2)	1001(2)	-41(2)	44
C2	215(2)	65(3)	757(2)	43
C3	1222(2)	320(3)	1340(2)	48
C3a	1357(2)	1564(3)	881(2)	48
C4	2071(2)	2339(4)	1143(3)	60
C5	2067(3)	3434(4)	641(3)	70
C6	1337(3)	3750(4)	-115(3)	73
C7	612(3)	2982(3)	-385(3)	61
C7a	632(2)	1867(3)	105(2)	46
C8	-343(2)	105(3)	1379(2)	45
C9	-845(2)	1151(3)	1372(2)	56
C10	-1319(2)	1247(4)	1993(3)	67
C11	-1268(2)	292(4)	2632(3)	69
C12	-773(3)	-756(4)	2660(3)	66
C13	-308(2)	-854(3)	2036(2)	56
C14	1428(2)	535(4)	2419(2)	62
C15	1809(2)	-739(4)	1207(3)	66
<i>Molecule II</i>				
N1	4809(2)	4999(2)	-749(2)	43
C2	5063(2)	3997(3)	-4(2)	40
C3	5950(2)	3401(3)	-49(2)	49
C3a	5963(2)	3952(3)	-986(2)	50
C4	6505(2)	3622(4)	-1496(3)	66
C5	6413(2)	4254(4)	-2342(3)	73
C6	5793(3)	5162(4)	-2671(3)	72
C7	5233(2)	5503(4)	-2183(2)	59
C7a	5346(2)	4875(3)	-1322(2)	48
C8	4375(2)	3040(3)	-91(2)	42
C9	3692(2)	2905(3)	-956(2)	52
C10	3069(2)	1976(3)	-1067(3)	59
C11	3116(2)	1168(3)	-329(3)	63
C12	3791(2)	1288(3)	531(3)	61
C13	4407(2)	2206(3)	633(2)	53
C14	5953(3)	1954(3)	-96(3)	71
C15	6753(2)	3846(4)	770(3)	66

observed at atom C3 bearing the two methyl groups. These two groups are symmetrically disposed on either side of the mean plane, at $-1.302(2)$ and $1.254(2)$ Å for C14 and C15, respectively. In the phenyl ring, the aromatic bond distances average 1.395 Å. As observed in the dimethylaminophenyl derivative [12], the two C9–C10 and C12–C13 bonds are clearly shorter than the other four phenyl bonds, while the two

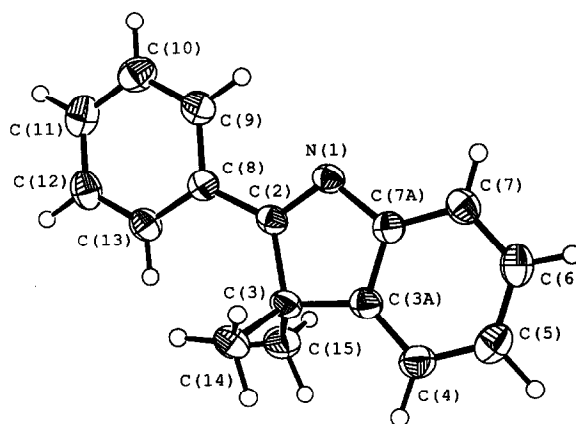


Fig. 1. Representation of the molecule and atomic numbering adopted for the monomer.

intracyclic angles, at C8 and C11, have values of $117.9(2)$ and $119.7(2)^\circ$, respectively; at the same time the other bond angles are all larger than 120° . These deviations, more pronounced in the case of the dimethylaminophenyl derivative, are discussed in ref. 35. There are no short contacts between neighboring molecules and hence the molecules are held in the crystal by van der Waals interactions only. The stereoview in Fig. 2 shows that, in the unit cell, the molecules are grouped in pairs and there are four such pairs, each in a different orientation. The two molecules in a pair are centrosymmetrically related and parallel to one another. One such pair is shown in projections parallel and perpendicular to the molecular plane in Fig. 3. The distance separating the molecular planes in a pair is 3.48 Å.

Dimer

The density indicates the presence of two crystallographically distinct moieties of the dimer in the asymmetric unit. In other words, there are two distinct half dimers, the other half of each dimer is generated by a center of symmetry. The two independent half molecules are referred to as molecule I and molecule II. Each dimer consists of two monomers linked by covalent bonds between atom N1 of one molecule to C2 of the other molecule, and vice versa, thus forming a four-membered ring. The dimer is shown by the stereopair in Fig. 4.

Table 5

Comparison of the intramolecular bond lengths and bond angles for the monomer $C_{16}H_{15}N$ and the dimer $C_{32}H_{30}N_2$

	Monomer		Dimer (X-ray)	
	X-ray	AMPAC	Molecule I	Molecule II
<i>Bond lengths (Å)</i>				
N1–C2	1.300(2)	1.322	1.495(4)	1.489(4)
N1–C7a	1.422(2)	1.424	1.414(5)	1.423(4)
N1–C2 ^a	3.564(2) ^b	—	1.514(4)	1.508(4)
C2–C3	1.546(2)	1.560	1.604(5)	1.605(5)
C2–C8	1.480(2)	1.464	1.505(5)	1.488(5)
C3–C3a	1.508(2)	1.519	1.535(5)	1.519(5)
C3–C14	1.553(2)	1.514	1.542(5)	1.536(5)
C3–C15	1.544(3)	1.514	1.533(5)	1.533(5)
C3a–C4	1.388(3)	1.379	1.372(5)	1.393(5)
C3a–C7a	1.399(2)	1.433	1.384(5)	1.373(5)
C4–C5	1.390(3)	1.403	1.379(6)	1.389(6)
C5–C6	1.398(3)	1.392	1.376(6)	1.363(6)
C6–C7	1.394(3)	1.392	1.382(6)	1.396(6)
C7–C7a	1.382(2)	1.392	1.384(5)	1.423(4)
C8–C9	1.412(2)	1.408	1.378(5)	1.397(5)
C8–C13	1.398(2)	1.402	1.398(5)	1.381(5)
C9–C10	1.387(3)	1.393	1.397(6)	1.386(5)
C10–C11	1.385(3)	1.394	1.372(6)	1.374(5)
C11–C12	1.392(3)	1.394	1.367(6)	1.384(6)
C12–C13	1.394(3)	1.394	1.390(6)	1.372(6)
<i>Bond angles (deg)</i>				
C2'...N1–C2	104.0(1) ^b	—	89.9(2)	91.0(3)
C2'–N1–C7a	—	—	121.9(3)	123.5(3)
C2–N1–C7a	107.5(1)	108.3	107.5(3)	107.9(2)
N1'...C2–N1	75.4(1) ^b	—	90.1(2)	89.0(3)
N1–C2–C3	113.1(1)	113.0	107.0(3)	106.1(2)
N1–C2–C8	119.9(1)	122.6	112.9(3)	114.2(3)
C3–C2–C8	126.2(1)	124.4	112.9(3)	113.3(3)
C2–C3–C3a	99.1(1)	100.0	100.4(3)	100.4(3)
C2–C3–C14	111.3(1)	112.1	114.2(3)	114.3(3)
C2–C3–C15	113.8(1)	112.1	112.4(3)	112.9(3)
C3a–C3–C14	110.0(1)	109.8	108.8(3)	109.4(3)
C3a–C3–C15	110.8(1)	109.8	112.4(3)	109.7(3)
C3–C3a–C4	131.8(2)	131.7	128.7(3)	127.8(3)
C3–C3a–C7a	108.1(1)	107.4	111.0(3)	111.8(3)
C4–C3a–C7a	120.1(2)	120.8	120.3(3)	120.4(3)
C3a–C4–C5	118.7(2)	118.4	120.4(4)	118.6(4)
C4–C5–C6	120.7(2)	120.9	119.4(4)	120.3(4)
C5–C6–C7	120.7(2)	121.4	121.4(4)	122.4(4)
C6–C7–C7a	118.1(2)	118.0	119.0(4)	116.5(4)
N1–C7a–C3a	111.4(1)	111.3	113.0(3)	112.0(3)
N1–C7a–C7	126.9(2)	126.3	126.8(3)	126.0(3)
C3a–C7a–C7	121.6(2)	120.4	119.9(3)	121.7(3)
C2–C8–C9	118.7(1)	119.4	120.2(3)	119.7(3)
C2–C8–C13	123.4(2)	122.2	121.3(3)	122.8(3)
C9–C8–C13	117.9(2)	118.4	118.3(3)	117.4(3)
C8–C9–C10	120.8(2)	120.6	121.1(3)	120.6(3)
C9–C10–C11	120.4(2)	120.3	119.2(4)	120.5(4)
C10–C11–C12	119.7(2)	119.5	121.1(3)	119.5(4)
C11–C12–C13	120.1(2)	120.4	119.6(4)	119.6(4)
C8–C13–C12	121.0(2)	120.7	120.7(3)	122.4(3)

^a Primed atoms correspond to the centrosymmetrically related second half of the dimer.^b In the case of the monomer, primed atoms refer to the nearest molecule in a pair.

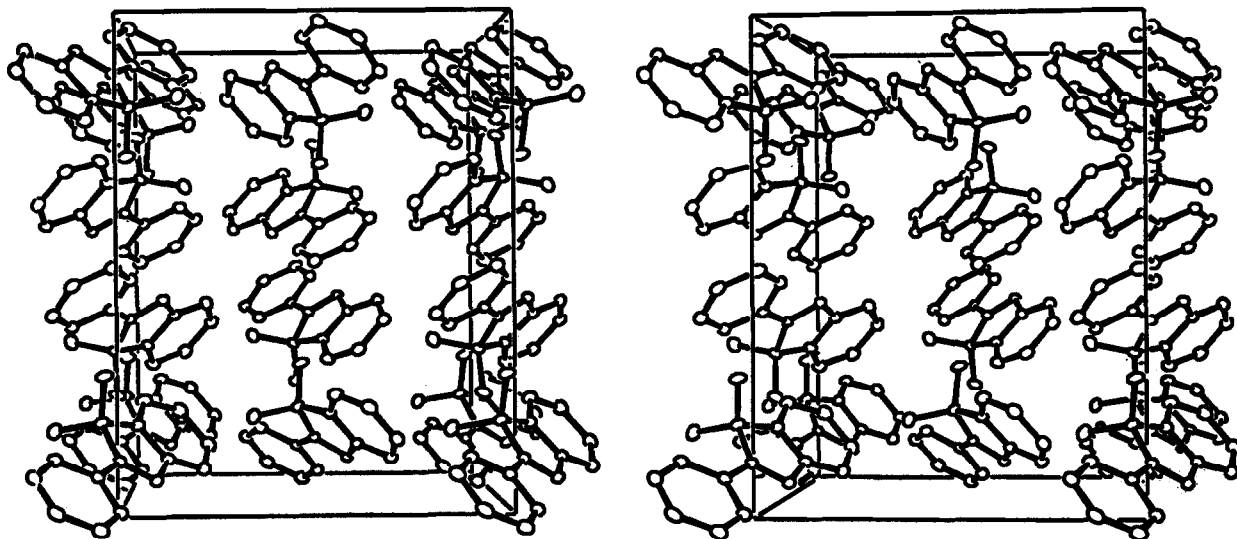


Fig. 2. Organization of the monomers in their unit cell.

The bond distances and angles of the dimer are compared in Table 5 with the corresponding quantities for the monomer. Obviously, there are some significant differences which are related to the dimerization. For instance, the N1–C2 bond length which was 1.300(2) Å is now 1.495(4)–1.498(4) Å in the dimer (in molecule I and molecule II, respectively). At the same time, the C2–C3 bond length changes from 1.546(2) Å to 1.604(4)–1.605(9) Å. The dimerization also affects some of the bond angles: N1–C2–C3 was 113.1(1)° in the monomer and is 106.1(2)–107.0(3)° in the dimer. The other bond angles around C2 are also

modified. Thus N1–C2–C8 and C3–C2–C8 with values of 119.9(1)° and 126.2(1)° in the monomer are now 112.9(3)–114.2(3)° and 112.9(3)–113.3(3)°, respectively, in the dimers. This is due to the fact that C2–N1, which was a double bond, is now a single bond.

The methyl groups, in either of the two half dimers, are not as symmetrically disposed with respect to the 3*H*-indole plane as they were in the monomer. The phenyl groups are planar and there are no recognizable deviations of the bond lengths from their respective averages.

The formation of the dimer gives rise to a planar

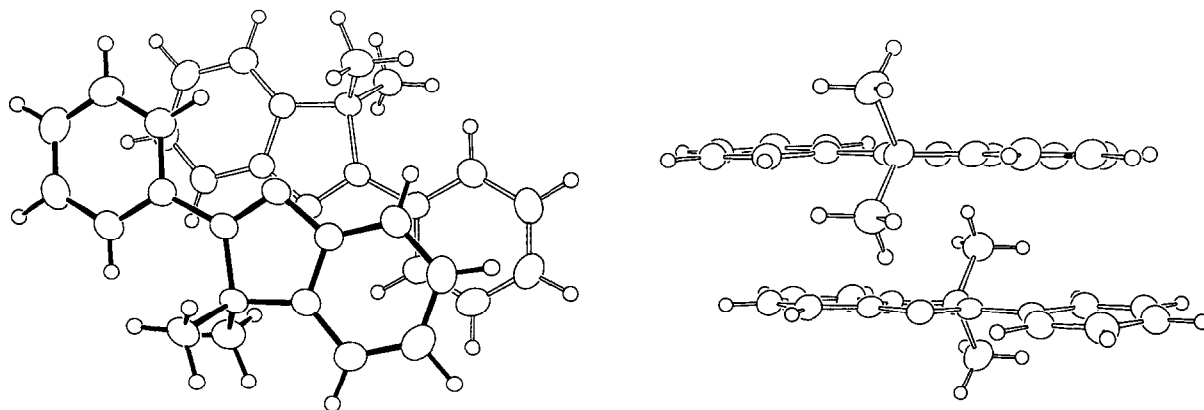


Fig. 3. Relative disposition of two molecules of the monomer: (a) top view; (b) side view.

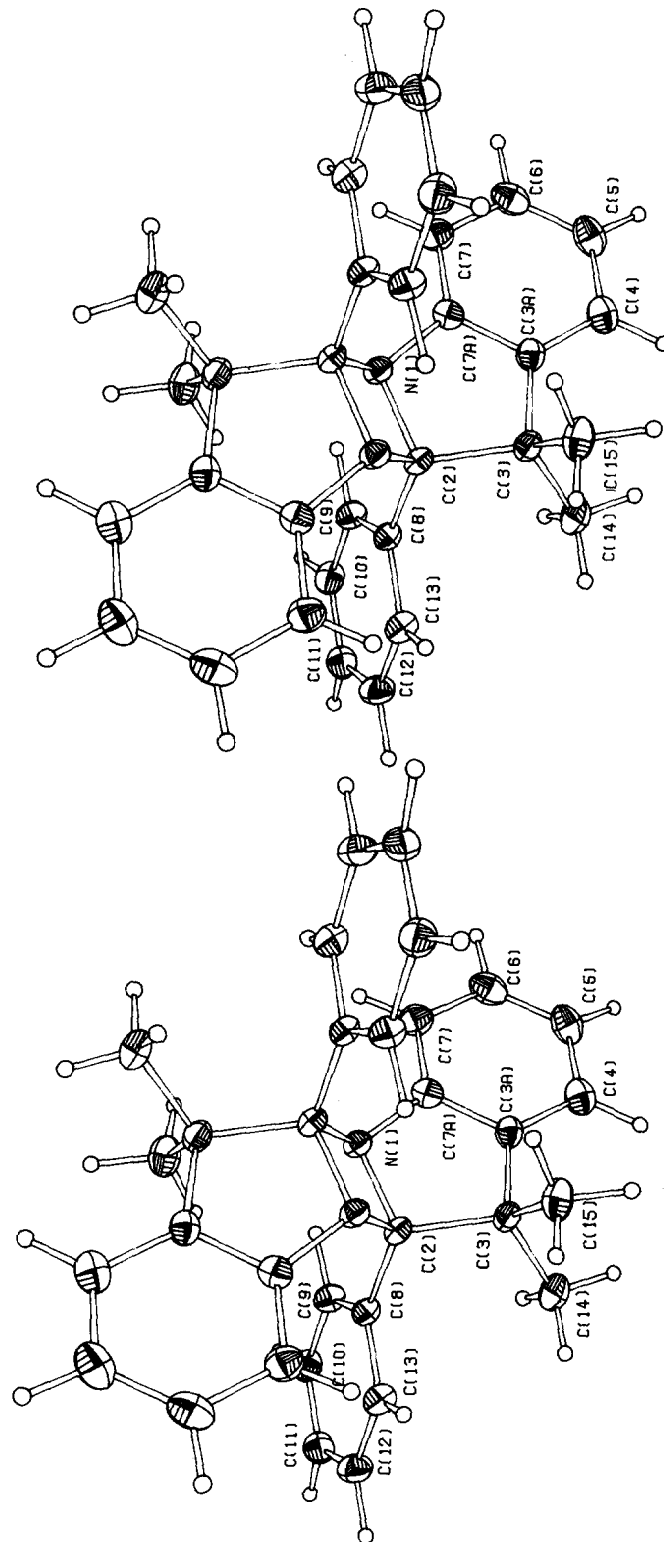


Fig. 4. Stereoview of the dimer and selected atomic numbering.

Table 6
The 3*H*-indole mean plane in the monomer and the dimer

Atom	Deviation from mean plane (Å)		
	Monomer	Dimer	
		Molecule I	Molecule II
N1	-0.011(1)	0.032(3)	-0.023(3)
C2	0.002(2)	-0.112(3)	0.146(3)
C3	0.008(2)	-0.051(4)	-0.090(3)
C3a	0.002(2)	0.029(4)	-0.040(4)
C4	-0.007(2)	-0.008(4)	0.032(4)
C5	-0.009(2)	-0.033(4)	0.059(4)
C6	0.005(2)	-0.041(4)	0.040(4)
C7	0.009(2)	-0.010(4)	-0.014(4)
C7a	0.004(2)	0.056(3)	-0.068(4)
C14 ^a	-1.302(2)	1.359(4)	1.002(4)
C15 ^a	1.254(2)	-1.117(3)	-1.461(4)

^a Atoms not included in the mean-plane calculation.

four-membered ring made up of N1, N1', C2 and C2'. The ring distances in the two half dimers are N1–C2 = 1.495(4) and 1.489(4) Å and N1–C2' = 1.514(4) and 1.508(4) Å, and the ring angles are C2'–N1–C2 = 89.9(2) and 91.0(3)° and N1–C2–N1' = 90.1(2) and 89.0(3)°. The 3*H*-indole group of atoms is not as planar as in the monomer (see Table 6). This is so because in the dimerization the N1–C2 has lost its double-bond character. The 3*H*-indole plane, such as it is, is at 123 and 131° from the four-membered ring plane,

while the planar phenyl rings are at 73 and 74° from the 3*H*-indole plane, for molecule I and molecule II, respectively. The relative disposition of the dimers in the unit cell is shown in Fig. 5.

In order to dimerize, the two monomer molecules forming a pair must be close enough and have a proper orientation (see Fig. 6). This is indeed the case because in the crystal structure of the monomer, the N1 and C2 atoms and their counterparts are 3.564(2) Å apart, while in the dimer the corresponding bond length is 1.514(2) and 1.508(2) Å for molecule I and molecule II, respectively. This implies that the two molecules must get closer by about 2 Å. There must also be a rotation of about 14°, because the angles C2–N1–C2' and N1–C2–N1' change from 104.6(1) to about 90°.

Semiempirical calculations

Ground-state calculations

The AM1 geometry optimization of **1** was performed, and the results are reported in Table 5. The AMPAC semiempirical method and the crystallography agree reasonably well with each other. Except for a couple of bonds (N1–C2 and C2–C8), all calculated bond lengths agreed quite well with the X-ray structure. The root-mean-square deviation for the bond lengths is 0.012 Å, including the two exceptions above. The agree-

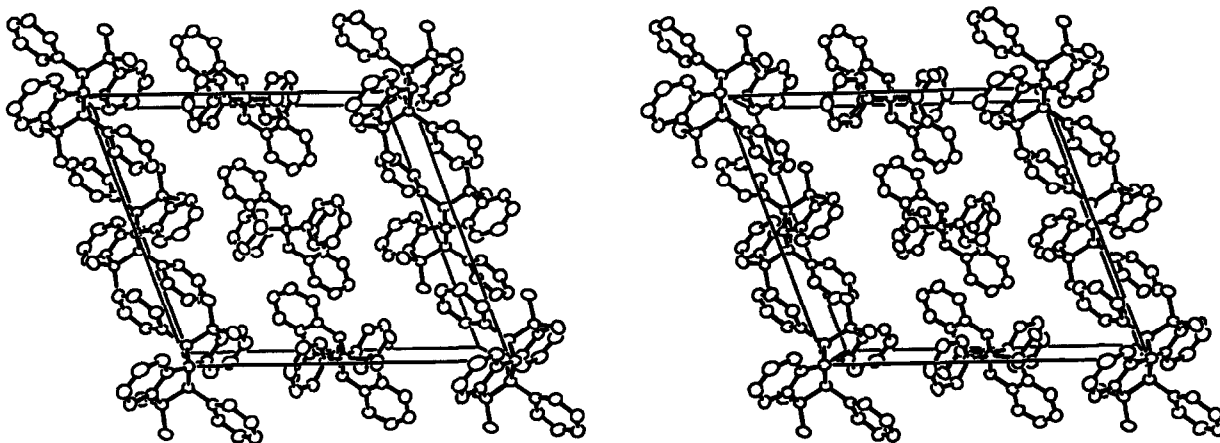


Fig. 5. Packing of the dimers in their unit cell.

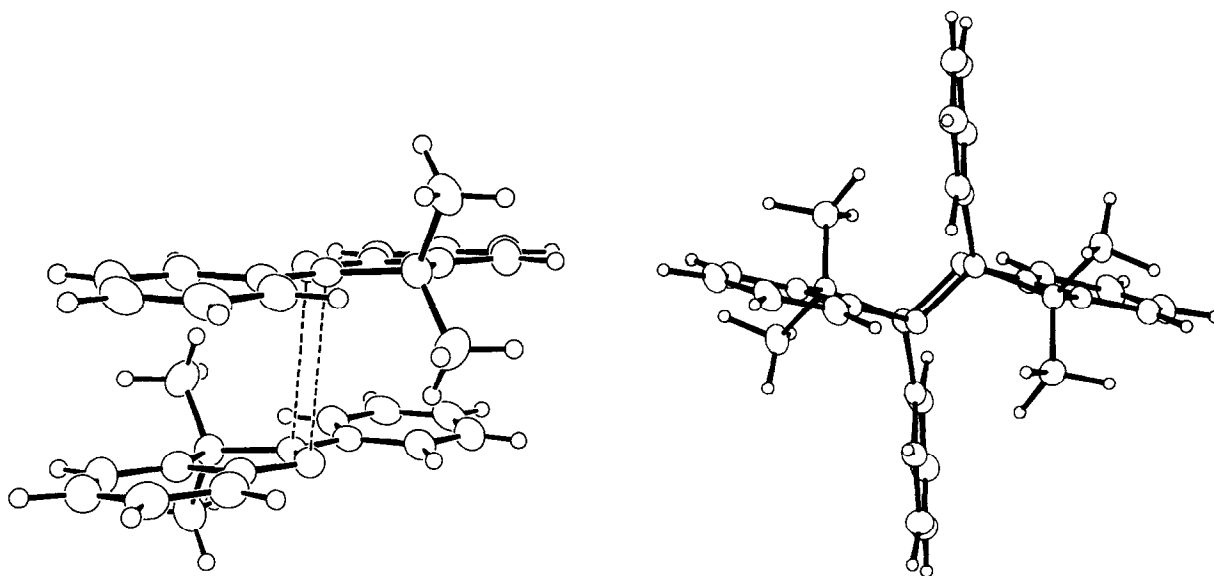


Fig. 6. Comparison of two neighboring monomers showing the bond formation and the resulting dimer.

ment is also very good for the angles with an average difference of 1° . On many occasions though, this agreement stops when one compares the torsional angles (tilt angles) between the two aromatic rings. It was shown that AMPAC calculates a nearly planar structure for the molecule where the X-ray shows dihedral angles between the two rings (see Table 7): N1–C2–C8–C9 and C3–C2–C8–C13 angles are about 5° . This discrepancy is corroborated by that observed in the bond lengths N(1)–C(2) and C(2)–C(8) which are shorter and longer respectively by about 0.02 \AA between the X-ray measurements and the calculated AMPAC values. Table 7 also shows that AMPAC predicts good dihedral angles when the ring torsion is not involved. It is not unusual that the X-ray data, because of the crystal packing involved, leads to smaller dihedral angles between rings than those calculated for the free molecule. The classic example is the biphenyl molecule which has a planar structure in the crystal, whereas the dihedral angle is about 45° in the vapor phase [36]. More recent examples have been given on hydroxyflavones [37]. It thus seems that the torsional angles are much underestimated by the AM1 geometry optimization.

The INDO/S semiempirical method was used to calculate the molecular energy at various tilt angles of the Ph_c ring, while the geometry of the remaining part of the molecule was kept unchanged and fixed by the AM1 method. Table 8 shows the results where all energies are compared with the minimum in the energy surface. One can see there is a broad range of angles around $\theta = 30^\circ$, with only shallow energy variation. The INDO/S prediction is that θ will fluctuate over a wide range of values between approximately 15 and 35° at room temperature ($kT = 25 \text{ meV}$), which obviously excludes both the calculated AMPAC and experimentally obtained X-ray values. This librational movement in the gas phase is obviously the interesting photo-physical property to follow in various environments if also present in the excited states.

Excited-state calculations

The INDO/S methodology was used to calculate the energy of the first singlet–singlet electronic transition along with the ground- and excited-state dipole moments using the AMPAC optimized geometry but varying the tilt angle θ . Table 8 shows, as expected for a $\pi\pi^*$ electronic transition delocalized throughout the entire molecule, that

Table 7
Comparison of the torsional angles in the monomer and the dimer

	Monomer		Dimer	
	X-ray	AMPAC	Molecule I	Molecule II
C3a–C4–C5–C6	–0.3(3)	–0.1	0.9(6)	–1.2(6)
C4–C5–C6–C7	0.6(3)		–0.7(6)	0.4(6)
C5–C6–C7–C7a	–0.2(3)		–1.2(6)	0.9(6)
C6–C7–C7a–C3a	–0.3(2)		2.9(6)	–1.4(5)
C7–C7a–C3a–C4	0.6(3)		–2.7(5)	0.6(6)
C7a–C3a–C4–C5	–0.2(3)	–0.1	0.8(6)	0.7(6)
C7–C7a–N1–C2	179.4(2)		–170.4(3)	169.6(3)
C3a–C7a–N1–C2	–1.1(2)		3.8(4)	–4.2(4)
C7a–N1–C2–C8	179.8(1)	179.9	116.3(3)	–114.6(4)
C7a–N1–C2–C3a	0.8(2)		–8.5(3)	11.0(3)
C2–C3–C3a–C4	179.4(2)		172.6(4)	–168.8(4)
C2–C3–C3a–C7a	–0.4(2)		–7.6(4)	11.0(4)
C3–C3a–C7a–N1	1.0(2)	0.1	2.9(4)	–5.0(4)
N1–C2–C3–C14	115.5(2)		125.8(3)	–130.5(3)
N1–C2–C3–C15	–117.8(2)		–110.1(3)	103.9(3)
C7a–C3a–C3–C14	–117.2(2)	–118.0	–127.9(3)	131.8(3)
C7a–C3a–C3–C15	119.3(2)	118.0	112.0(3)	–108.1(3)
N1–C2–C8–C9	–3.9(2)	0.1	–19.0(4)	18.8(4)
N1–C2–C8–C13	175.0(2)	179.9		
C3–C2–C8–C13	–6.0(3)		–71.5(4)	72.7(4)
C8–C2–C3–C15	–63.4(2)		0.9(4)	–4.4(4)
C8–C2–C3–C14	63.3(2)		125.0(3)	–130.1(3)

increasing the dihedral angle shifts the $\pi\pi^*$ transition to the blue region of the spectrum and decreases the excited state dipole moment following a decrease in the charge delocalization between the two chromophoric moieties. Table 8 also shows that the minimum in the potential energy surface for the S_1 state is a little shifted to a lower angle (about 15°) compared with the ground state, but this shift is not spectacular (less than 10°). However, the excited state energy surface is much steeper than the ground state surface. Let us now compare these theoretical predictions with the spectroscopic results obtained.

Spectroscopy

Electronic spectroscopy

All the experimental quantities needed for the discussion in the present paper are displayed in

Table 9. The order of the solvents used in the Table follows their increasing macroscopic viscosities. It was shown that an excellent mirror-image relationship [12,13] exists between the

Table 8

Energy and dipole moment variations of the ground (S_0) and first electronic state (S_1) of molecule 1 as a function of the tilt angle (θ) of the Ph_c ring as calculated by INDO/S

θ (deg)	$E_{S_0}^a$ (meV)	$\Delta E_{S_0-S_1}$ (cm^{-1})	E_{S_1} (eV)	μ_{S_0} (D)	μ_{S_1} (D)
0	83	32 399	4.0995	3.5	10.5
15	20	32 615	4.0632	3.6	10.4
30	0	33 148	4.1093	3.6	9.9
45	125	33 867	4.3242	3.6	8.7
60	231	36 463	4.7513	3.7	6.9
75	274	37 854	4.9666	3.7	5.9
90	283	38 211	5.0199	3.7	5.6

^a Relative values compared to the energy minimum.

Table 9
Spectroscopic and photophysical parameters of molecule 1 at 298 K

Solvent	n	D	η (cp)	$\bar{\nu}_A^a$ (cm^{-1})	$\bar{\nu}_F^a$ (cm^{-1})	ϕ_F ($\times 10^4$)	$k_F^{t,b}$ ($\times 10^{-8} \text{ s}^{-1}$)	τ_F^c (ps)	k_{nr}^d ($\times 10^{-10} \text{ s}^{-1}$)
Perfluorohexane	1.252	1.568	0.13	33 670	25 910	2.4	2.4	1.0	100
Diethylether	1.352	4.34	0.24	33 110	25 100	4.2	3.1	1.4	74
Acetonitrile	1.344	37.5	0.35	33 110	25 190	5.1	2.6	2.0	51
<i>n</i> -Heptane	1.387	1.924	0.4	33 110	25 580	4.6	2.9	1.6	63
Methanol	1.331	32.6	0.55	33 220	24 690	6.3	2.5	2.5	40
Tetrahydrofurane	1.407	7.58	0.55	32 900	24 880	6.4	3.2	2.0	50
<i>n</i> -Decane	1.409	1.991	0.93	33 000	26 040	12	3.3	3.6	28
Water (pH = 9.5)	1.333	80.2	1.00	33 330	23 870	11	2.1	5.2	19
1,4-Dioxane	1.439	2.21	1.44	33 000	25 000	9.8	3.0	3.3	31
<i>n</i> -Dodecane	1.422	2.002	1.51	32 900	26 740	14	3.6	3.9	26
<i>n</i> -Tetradecane	1.429	2.042	2.18	32 900	25 970	15	3.2	4.7	21
<i>n</i> -Propanol	1.384	20.33	2.26	33 000	25 510	15	2.9	5.2	19
<i>n</i> -Butanol	1.399	17.51	2.95	32 900	24 810	16	2.7	5.9	17
<i>n</i> -Hexadecane	1.435	2.1	3.34	32 900	27 100	17	3.5	4.9	21
<i>n</i> -Pentanol	1.409	13.9	4	32 900	24 630	20	2.7	7.4	14
<i>n</i> -Hexanol	1.418	13.3	4.59	32 900	25 380	27	2.8	9.6	10
Ethyleneglycol	1.432	37.7	26.1	32 680	24 630	105	3.1	34	2.9
Glycerol	1.475	42.5	1412	32 470	24 330	1150	2.2	523	0.2

^a Measured at the peak maxima.

^b k_F^t was obtained using the Strickler and Berg relationship [30].

^c Values calculated from $\tau_F = \phi_F/k_F^t$.

^d Values calculated from $k_{nr} = k_F^t \phi_F^t (1 - \phi_F)$.

corrected absorption and fluorescence spectra of 1 in all these solvents, corroborating the fact discussed above (INDO/S) that the geometry in both states is practically identical. This fact, together with some others discussed elsewhere [17], allows us to predict the fluorescence lifetime by using the assumption that the theoretical fluorescence decay rate constant ($k_F^{(t)}$) is identical to the fluorescence decay rate constant (k_F). Moreover, a plot of $\log(k_F/n^3)$ versus $\log(\bar{\nu}_F)$ in all solvents was shown to give a straight line with a slope of nearly 3 (2.8), which indicates that the state responsible for the fluorescence emission in all these solvents is not much different in geometry and charge delocalization than the ground electronic state [17].

In order to evaluate the energy of the first electronic transition in the gas phase, we used the method previously described [12] which consists in measuring the absorption spectra

of 1 in a series of non-polar solvents from perfluorohexane to *n*-hexadecane (Table 9). A plot of $\bar{\nu}_A$ versus $f(n^2)$, the polarizability function defined as

$$f(n^2) = 2(n^2 - 1)/2n^2 + 1 \quad (1)$$

where n is the refractive index of the solvent, gives rise to a good linear correlation ($r^2 = 0.992$):

$$\bar{\nu}_A = 35230(\pm 30) - 5600(\pm 260)f(n^2) \quad (2)$$

This shows that extrapolation of the $f(n^2)$ plot to $n = 1$ (gas phase) gives a value of $\bar{\nu}_A$ (about $35\,000 \text{ cm}^{-1}$) which compares with that calculated by INDO/S for a torsional angle of approximately 50° (see Table 8) for the ground electronic state configuration.

We have also recently shown [17], by using various solvatochromic methods on the data reported in Table 9, that the optimized values of the ground-

and excited-state dipole moments are 3.8 and 7.8 D, respectively, with a negligible molecular polarizability. This experimental result which is entirely independent of the energy also confirms a value of approximately 50° for the dihedral angle in molecule **1** (see Table 8).

We then conclude that AMPAC, although good in optimizing the rest of the geometry, failed in optimizing the dihedral angle of molecule **1**. INDO/S has been used to evaluate electronic S_0 – S_n transition data of molecule **1** at the AMPAC optimized geometry but with a dihedral angle of 45° . The results are combined in Table 10. One can see that all electronic transitions are of the $\pi\pi^*$ type and polarized in the xy plane except the $S_4 \leftarrow S_0$ transition which is of the $n\pi^*$ type and polarized out of plane. The first two electronic transitions have about the same oscillator strength and are separated by only 2000 cm^{-1} giving rise to a strong Herzberg–Teller vibronic coupling [12]. The consequence of this is the observation of only one absorption band in solution (see Table 9) in the electronic spectra of the molecule and also the occurrence of a fluorescence band which has a mirror-symmetry relationship with its absorption counterpart as discussed above. The total oscillator strength (0.72) predicted for the

first electronic band system of molecule **1** is a little less than that predicted for DM3H (1.1) [12]. This is confirmed by comparison of the integrated absorption spectra of both molecules in non-polar solvents where the theoretical radiative decay rates ($k_F^{(i)}$) are equal to $2.9 \times 10^8\text{ s}^{-1}$ (Table 9) and $3.3 \times 10^8\text{ s}^{-1}$ for **1** and DM3H, respectively [12]. The second band system in molecule **1** is centered at 44000 cm^{-1} with an oscillator strength about half of that of the first band system. This should correspond to the $S_6 \leftarrow S_0$ transition predicted by INDO/S to appear at 44800 cm^{-1} with an f value of 0.26 (Table 10). These results show that the AMPAC optimized geometry with a dihedral angle of around 45° fully interprets all the spectroscopic results obtained on molecule **1**.

Photophysics

Table 9 shows that the fluorescence quantum yields and lifetimes of molecule **1** are quite sensitive to the viscosity of the macroscopic solvent. A regular increase in those parameters is observed when the viscosity of the solvent increases. What makes molecule **1** so interesting as a viscosity fluorescence probe, though, is the fact that contrary to more highly substituted polar analogs in the series [12,13]

Table 10

Electronic transitions obtained by the INDO/S semiempirical method for molecule **1** at the AMPAC optimized geometry but with a dihedral angle of 45°

Electronic transitions	ΔE (cm^{-1})	f	MO	Character	Localized/ delocalized	Transition dipole axis ^a	μ^b (D)
$S_1 \leftarrow S_0$	33867	0.4054	43 \leftarrow 42	$\pi\pi^*$	Deloc.	y	8.6
$S_2 \leftarrow S_0$	35632	0.3175	46 \leftarrow 42	$\pi\pi^*$	Deloc.	xy	7.9
$S_3 \leftarrow S_0$	36509	0.0008	43 \leftarrow 39	$\pi\pi^*$	Deloc.	xy	3.8
$S_4 \leftarrow S_0$	37022	0.0060	43 \leftarrow 38	$\pi\pi^*$	Deloc.	z	4.2
$S_5 \leftarrow S_0$	44098	0.0258	45 \leftarrow 42	$\pi\pi^*$	Loc. (In)	y	4.7
$S_6 \leftarrow S_0$	44795	0.2627	43 \leftarrow 41	$\pi\pi^*$	Deloc.	xy	7.1
$S_7 \leftarrow S_0$	46005	0.0473	43 \leftarrow 40	$\pi\pi^*$	Deloc.	xy	5.1
$S_8 \leftarrow S_0$	47104	0.1348	44 \leftarrow 42	$\pi\pi^*$	Deloc.	xy	6.1
$S_9 \leftarrow S_0$	48149	0.1852	47 \leftarrow 42	$\pi\pi^*$	Deloc.	xy	6.5

^a The long molecular axis is y .

^b The ground state dipole moment (μ_0) was calculated to be 3.6 D.

or for triphenylmethane [38] and rhodamine dyes [39], the solvent polarity does not affect the viscosity correlation. FH type correlations with viscosity (in centipoise) including all the solvents in Table 9 were obtained with both the quantum yields and lifetimes [17]:

$$\phi_F = 9.4(\pm 0.3) \times 10^{-4} \eta^{2/3} (\text{cP}) \quad (3)$$

$$\tau_F = 3.3\text{ps}(\pm 0.2) \eta^{2/3} (\text{cP}) \quad (4)$$

These excellent linear correlations involving solvents of different polar, hydrogen bonding and viscosity properties support the idea that the excited state dynamics of **1** is independent of the free volume of each particular solvent. The solvent polarity and/or hydrogen bonding capability does not affect the mechanism responsible for the internal rotation of the Ph_c ring.

Molecule **1** could then be used as an excellent viscosity probe for heterogeneous systems and polymers in a very large range of viscosities. However, it might also be used to gain more insight into the applicability of recent theories on the dynamics of negligible to moderately low energy barrier reactions in solutions [17].

Concluding remarks

The ground state conformation and geometry of 2-phenyl-3,3-dimethyl-3*H*-indole (**1**) and its dimer were characterized by crystallographic measurements. Many of the bond lengths and angles of **1** are drastically changed in the dimer where the C=N double bond disappears making the electron delocalization between both phenyl and indolic chromophores no longer feasible. The monomer is then obviously a better candidate to be used as a molecular sensor of polarity and/or viscosity in homogeneous and heterogeneous systems. Both crystallographic measurements and AMPAC-AM1 geometry optimization showed good agreement with each other except for the dihedral angle between the Ph_c ring and the indolic moiety which was shown, by INDO/S calculations coupled to spectroscopic measurements, to be under-

estimated. Contrary to the *p*-dimethylamino Ph_c ring substituted compound (DM3H), the solid-state structure of **1** as determined by X-ray diffraction does not represent the most stable conformation available to the molecule in solution at room temperature. We have shown that the Ph_c ring can librate within a range of about 20° around the equilibrium dihedral angle of approximately 45° at room temperature in the ground electronic state of the molecule. This equilibrium geometry is shifted to lower angle by approximately 10° in the first excited singlet state, but not enough to affect the good mirror-image relationship observed between the absorption and fluorescence spectra of molecule **1** in the various environments studied in this work. It was shown that owing to this librational motion the nonradiative fluorescence decay rate constant entirely controls the excited-state dynamics of molecule **1** in solution. More importantly, these excited-state dynamics are independent of specific interactions with protic solvent and also of the free volume of each particular solvent, being influenced only by the viscous drag (macropolarity) of each solvent considered.

Acknowledgments

We would like to express our deep gratitude to Emeritus Professor Camille Sandorfy who pioneered three important physical chemistry domains in the early 1960s here at the Université de Montréal: quantum chemistry, electronic and infrared spectroscopy. These domains have developed, throughout the years, to an extent where eight Faculty members are now working in these fields of research.

We gratefully acknowledge the financial assistance of the Natural Sciences and Engineering Research Council of Canada and the Fonds FCAR (Québec) in the form of grants.

References

- 1 J.R. Bolton, N. Mataga, G. McLendon (Eds.), Electron

- Transfer in Inorganic, Organic and Biological Systems, Advances in Chemistry Series 228, American Chemical Society, Washington, DC, 1991.
- 2 F. Brisse, G. Durocher, S. Gauthier, D. Gravel, R. Marquès, C. Vergelati and B. Zelent, *J. Am. Chem. Soc.*, 108 (1986) 657.
B. Zelent, P. Messier, D. Gravel, S. Gauthier and G. Durocher, *J. Photochem. Photobiol.*, 40 (1987) 145.
B. Zelent, P. Messier, S. Gauthier, D. Gravel and G. Durocher, *J. Photochem. Photobiol.*, 52 (1990) 165.
D. Gravel, S. Gauthier, F. Brisse, S. Raymond, M. D'Amboise, P. Messier, B. Zelent and G. Durocher, *Can. J. Chem.*, 68 (1990) 908.
T. Ganguly, D.K. Sharma, S. Gauthier, D. Gravel and G. Durocher, *J. Phys. Chem.*, 96 (1992) 3757.
 - 3 H. Zeng, M. Sow, M.A. Séguin and G. Durocher, *J. Phys. Chem.*, in press.
 - 4 R.P. Haugland, *Handbook of Fluorescent Probes and Research Chemicals*, Molecular Probes Inc., Eugene, OR, USA, 1989.
G.S. Beddard and M.S. West, *Fluorescent Probes*, Academic Press, New York, 1981.
 - 5 P.M. Bayley and R.E. Dale (Eds.), *Spectroscopy and the Dynamics of Molecular Biological Systems*, Academic Press, New York, 1986.
R.E. Dale, L.A. Chen and L. Brand, *J. Biol. Chem.*, 252 (1977) 7500.
J.R. Lakowicz, *J. Biochem. Biophys. Methods*, 2 (1980) 91.
C.E. Kung and J.K. Reed, *Biochemistry*, 25 (1986) 6114.
 - 6 C.J. Drummond, F. Grieser and T.W. Healy, *Faraday Discuss. Chem. Soc.*, 81 (1986) 95.
 - 7 M. Belletête and G. Durocher, *J. Colloid Interface Sci.*, 134 (1990) 289.
M. Belletête, M. Lachapelle and G. Durocher, *J. Phys. Chem.*, 94 (1990) 5337, 7642.
 - 8 D. Anwand, F.W. Müller, B. Strehmel and K. Schiller, *Makromol. Chem.*, 192 (1991) 1981.
 - 9 G.C. Walker, E. Akesson, A.E. Johnson, N.E. Levinger and P.F. Barbara, *J. Phys. Chem.*, 96 (1992) 3728.
E. Akesson, G.C. Walker and P.F. Barbara, *J. Chem. Phys.*, 95 (1991) 4188.
K. Tominaga, G.C. Walker, W. Jarzeba and P.F. Barbara, *J. Phys. Chem.*, 95 (1991) 10475.
W. Jarzeba, G.C. Walker, A.E. Johnson and P.F. Barbara, *Chem. Phys.*, 152 (1991) 57.
 - 10 Z.R. Grabowski, K. Rotkiewicz, A. Siemiarz, D.J. Cowley and W. Baumann, *Nouv. J. Chim.*, 3 (1979) 443.
W. Rettig, W. Majenz and R. Lapouyade, *J. Photochem. Photobiol. A: Chem.*, 62 (1992) 415.
J. Dobkowski, W. Rettig, C. Rullière, J. Waluk and W. Yang, *Radiat. Phys. Chem.*, 39 (1992) 149.
W. Baumann, H. Bischof, J.C. Fröhling, C. Buttinger, W. Rettig and K. Rotkiewicz, *J. Photochem. Photobiol. A: Chem.*, 64 (1992) 49.
W. Rettig, *Ber. Bunsenges Phys. Chem.*, 95 (1991) 259.
 - 11 A. Popowycz, M.Sc. Thesis, University of Montreal, 1992.
 - 12 M. Lachapelle, M. Belletête, M. Poulin, N. Godbout, F. Legrand, A. Héroux, F. Brisse and G. Durocher, *J. Phys. Chem.*, 95 (1991) 9764.
 - 13 M. Belletête and G. Durocher, *J. Phys. Chem.*, 96 (1992) 9183.
 - 14 R.S. Sarpal, M. Belletête and G. Durocher, *J. Phys. Chem.*, 97 (1993) 5007.
 - 15 A. Héroux, M.Sc. Thesis, University of Montreal, 1992.
 - 16 Th. Förster and G. Hoffmann, *Z. Phys. Chem.*, 75 (1971) 63.
 - 17 M. Belletête, R.S. Sarpal and G. Durocher, *Chem. Phys. Lett.*, 201 (1993) 145.
 - 18 W.C. Still, M. Kahn and A. Mitra, *J. Org. Chem.*, 43 (1978) 2923.
 - 19 F.J. Evans, G.G. Lyle, J. Watkins and R.E. Lyle, *J. Org. Chem.* 27 (1962) 1553.
F.J. Evans and R.E. Lyle, *Chem. Ind. (London)*, (1963) 986.
 - 20 H.M. Kissman, D.W. Farhsworth and B. Witkop, *J. Am. Chem. Soc.*, 74 (1952) 3948.
B. Witkop, J.B. Patrick and H.M. Kissman, *Chem. Ber.*, 85 (1952) 949.
H.M. Leuchs, A. Heller and A. Hoffman, *Chem. Ber.*, 62 (1929) 877.
 - 21 M. Yoshida, H. Minato and M. Kobayashi, *Chem. Lett.*, 1097 (1976).
E. Denecke, K. Müller and T. Bluhm, *Org. Magn. Reson.*, 18 (1982) 68.
 - 22 The programs used here were modified versions of: NRC-2, data reduction; NRC-10, bond distances and angles; NRC-22, mean planes; FORDAP, Fourier and Patterson maps (A.Zalkin); MULTAN 80, multi-resolution program; NUCLS, least-squares refinement; ORTEP, stereodrawings [19–21].
 - 23 F.R. Ahmed, S.R. Hall, M.E. Pippy and C.P. Huber, *J. Appl. Crystallogr.*, 6 (1973) 309.
 - 24 P. Main, S.J. Fiske, S.E. Hull, L. Lessinger, G. Germain, J.P. Declercq and M.M. Woolfson, MULTAN 80. A System of Computer Programs for the Automatic Solution of Crystal Structures from X-ray Diffraction Data, University of York/University of Louvain, 1980.
 - 25 C.K. Johnson, ORTEP Report ORNL-3794, Oak Ridge National Laboratory, TN, 1965.
 - 26 The hydrogen atom coordinates, anisotropic temperature factors, least-squares planes and the tables of observed and calculated structure factors have been deposited with B.L.L.D. as Supplementary Publication number SUP 26472 (31 pages).

- 27 D.T. Cromer, and J.R. Mann, *Acta Crystallogr., Sect. A*, 24 (1968) 321.
- 28 R.F. Stewart, E.R. Davidson and W.T. Simpson, *J. Chem. Phys.*, 42 (1965) 3175.
- 29 J.C. Tai and N.L. Allinger, *J. Am. Chem. Soc.*, 110 (1988) 2050.
- 30 M.J.S. Dewar, E.G. Zoebisch, E.F. Healy and J.J.P. Stewart, *J. Am. Chem. Soc.*, 107 (1985) 3902.
- 31 J. Ridley and M.C. Zerner, *Theor. Chim. Acta*, 32 (1973) 111.
C. Forber and M.C. Zerner, *J. Am. Chem. Soc.*, 107 (1985) 5884.
- 32 M. Belletête and G. Durocher, *J. Photochem.*, 21 (1983) 251.
- 33 M. Belletête and G. Durocher, *J. Phys. Chem.*, 93 (1989) 1793.
- 34 S.J. Strickler and R.A. Berg, *J. Chem. Phys.*, 37 (1962) 814.
- 35 A. Domenicano, A. Vaciago and C.A. Coulson, *Acta Crystallogr., Sect. B*, 31 (1975) 1630.
- 36 A. Almendinger, O. Bastiansen, L. Fernholt, B.N. Cyvin, S.J. Cyvin and S.J. Samdal, *J. Mol. Struct.*, 128 (1985) 59.
- 37 B. Dick, *J. Phys. Chem.*, 94 (1990) 5752.
- 38 M. Vogel and W. Rettig, *Ber. Bunsenges Phys. Chem.*, 91 (1987) 1241.
- 39 C.J. Tredwell and A.D. Osborne, *J. Chem. Soc., Faraday Trans. 2*, 76 (1980) 1627.
A.D. Osborne, *J. Chem. Soc., Faraday Trans. 2*, 76 (1980) 1638.